

Full paper

Design and Development of a Novel Robotic Platform for Neuro-Robotics Applications: the NEURobotics ARM (NEURARM)

**Emanuele Cattin^a, Stefano Roccella^a, Nicola Vitiello^a, Irene Sardellitti^a,
Panagiotis K. Artemiadis^b, Pierpaolo Vacalebri^a, Fabrizio Vecchi^{a,*},
Maria Chiara Carrozza^a, Kostas J. Kyriakopoulos^b and Paolo Dario^a**

^a ARTS Lab, Scuola Superiore Sant'Anna, Polo Sant'Anna Valdera, Viale Rinaldo Piaggio 34, 56025 Pontedera (PI), Italy

^b Control Systems Laboratory, Mechanical Engineering Department, National Technical University of Athens, 9 Heroon Polytechniou Street, Athens 157 80, Greece

Received 24 October 2006; accepted 28 May 2007

Abstract

This paper presents the NEURARM, a novel robotic platform specifically designed for performing joint experiments between neuroscience and robotics. The NEURARM replicates the main functions and characteristics of the human arm during the execution of planar movements for reaching and catching a moving object. The NEURARM is a 2-d.o.f. planar robotic platform actuated by means of four linear hydraulic actuators and four cables integrated in agonist–antagonist configuration. The first version of a non-linear spring that will be integrated in series with the actuator has been developed and tested. The main components of the sensory system are four tension sensors on the cables, two angle sensors in the joints, and linear potentiometers and pressure sensors on the pistons. The paper presents the design methodology, the developed components and system, and the experimental characterization of the NEURARM. The available data demonstrate qualitatively that the design is appropriate, that the NEURARM is able to replicate the required maximum kinematics performance and that real joint experiments with neuroscientists can start.

© Koninklijke Brill NV, Leiden and The Robotics Society of Japan, 2008

Keywords

Biorobotics, neuro-robotics, anthropomorphic, robotic arm, cable-driven robot, agonist-antagonist actuation

* To whom correspondence should be addressed. E-mail: fabrizio.vecchi@arts.sssup.it

1. Introduction

The catching task can be considered as a benchmarking task for the design of an advanced neuro-robotic platform able to mimick the human arm. The catching task can be also considered as a prototypical task, because it is well known and studied in neuroscience, and it involves different skills related to perception, action and prediction processes [1, 2]. A number of research groups developed anthropomorphic robotic arms for neuro-robotic applications. Hannaford's Anthroform Biorobotic Arm [3] is a good example of a neuro-robotic platform matching the anthropomorphic requirements because it was developed to study spinal circuits. The Dexter Arm [4, 5] is an 8-d.o.f. anthropomorphic cable-driven robotic arm. This robotic arm was used for assessing innovative bio-inspired neuro-controllers [6], but it is too slow to perform catching tasks (0.2 m/s velocity); moreover, mass and inertia of the links are greater than those of the human model. DLR Light Weight Robot III is a 7-d.o.f. electric actuated robotic arm [7]. Due to the payload/weight ratio and high dynamic performance, the DLR arm can be considered as a safe robot. The Whole Arm Manipulator (WAM) is a 4/7-d.o.f. high-performance cable-driven robot arm [8, 9]. Due to the high performance of the WAM arm, catching experiments were carried out [10]. However, the DLR LWR III and the WAM robotic arms are not anthropomorphic, and are not driven by antagonistic actuation that is a fundamental property to study motor control paradigms. This paper presents the NEUROBOTICS ARTS Lab robotic arm platform (NEURARM) specifically designed and developed to imitate the human arm in performing planar catching and reaching tasks. This paper presents the biomechatronic design, the related engineering solutions of the NEURARM and the experimental results of the assessment tests.

2. Biomechatronic Design Approach

The musculoskeletal structure is intrinsically redundant with its 9-d.o.f. and its multiple muscles acting on each joint (12 muscles in total with 25 branches) [11]. The natural motor control strategies are still not well known due to the complexity of the human arm.

The design approach followed in this work is aimed at replicating some of the functions of the human arm to assess natural motor control theories and hypotheses. For that reason some concentrated parameters were adjusted according to the different experimental protocols to provide repeatable and adjustable experimental conditions.

The scheme depicted in Fig. 1 describes the main phases in the biomechatronic design of the NEURARM.

In particular, the design process of the NEURARM started with the observation and analysis of the human arm during the execution of a reference task. Neuroscientists have agreed that the interception with a moving object [12] is a suitable and challenging benchmarking task for a robotic platform aimed at emulating the hu-

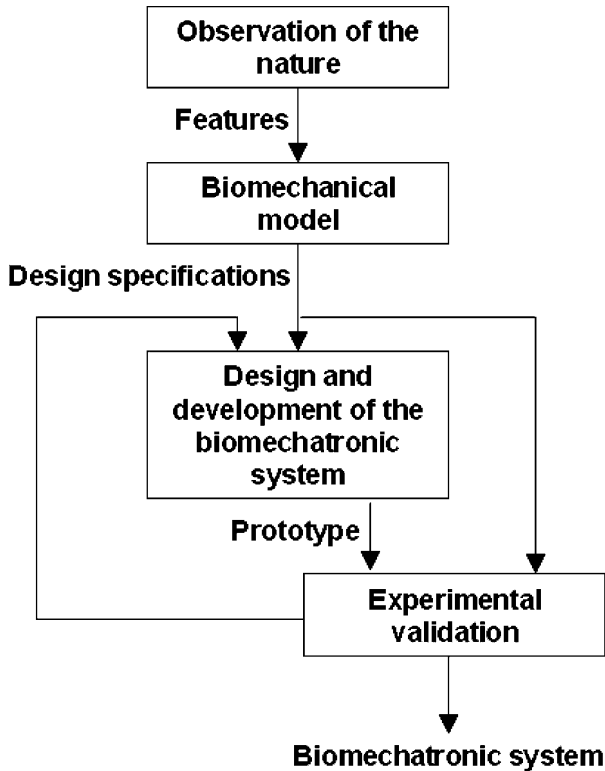


Figure 1. The biomechatronic design approach scheme: (1) the features of the desired system are defined according to the observation of nature, (2) the features are used to implement the biomechanical model that will be used to define the design specifications of the biomechatronic system (3) that will be designed, developed, (4) validated and, in case, redesigned.

man arm from a functional point of view. The main features of the human system considered in the design process were:

- Anthropometric size and inertial parameters of each limb segment [13, 16].
- Tendon transmission between the muscles and the segments [14, 16, 17].
- Non-linear behavior of the muscles [14–16, 18].
- Agonistic–antagonistic and multi-joint configuration of the muscles [14, 16, 19–21].
- Tuning of the muscle contraction force through neural activation signals [22, 24].
- Versatility in changing muscles synergies [14, 15, 25].

- Functions of the proprioceptive and exteroceptive sensory system (i.e., muscles spindles, joint receptors and Golgi tendon organs, tactile mechanoreceptors) [26, 29].
- Adjustable mechanical impedance [31, 34].

According to the biomechatronic design approach, even if there are no mechanical components able to imitate their biological counterparts, it is possible to focus the design on the functional emulation of the human arm and the relevant features outlined above. Therefore, each module was aimed at reproducing the functional behavior of the corresponding biological one. The next section presents the evaluation of the human arm performance during the execution of the reference task and the resulting biomechanical model used to define the design specifications of the NEURARM actuation system. In the following sections, each module of the biomechatronic system is described. Moreover, experimental results are presented and discussed.

3. Biomechanical Model of the Human Upper Limb

In order to develop an artificial arm able to achieve human arm performance, the measurement of human arm parameters during the task is essential [35]. Kajikawa *et al.* developed an experimental apparatus for the acquisition of human behavior during the planar catching of an object using spontaneous and pre-programmed protocols. Among other interesting results on the quantitative value of the hand velocity and acceleration, they found that the catching trajectory is next to a straight line between the starting point and the caught object. This is an important result because it is the basic assumption for the robotic arm design and for the preliminary development of its control algorithms. However, Kajikawa *et al.*'s apparatus was based on the use of a motorized object so the experimental trials could be influenced by the inertia of the actuation and transmission systems. Therefore, we designed a platform to perform catching tasks with a new experimental set-up where the object is free to move with higher velocities up to 1.5 m/s.

3.1. Experimental Apparatus Protocol

The experimental apparatus was intended to study the catching task of a moving object in the plane (see Fig. 2). The human arm movement was constrained in the plane and a predefined straight trajectory was imposed to the object. In this way the experimental conditions for repeatable and predefined tasks were obtained. The object could move along straight lines on the horizontal plane at different velocities (0.5, 1.0 and 1.5 m/s) that could be pre-defined. The Fastrack Polhemus Motion Capture System was used to acquire the human arm motion during the catching task. Four position sensors were placed, respectively, on the right shoulder, elbow, wrist and hand. The acquisition sample rate was 30 Hz.

The subject started from a pre-defined resting position (see Fig. 2), then stopped the slider moving in front of him on a straight line and finally grasped the cylindrical

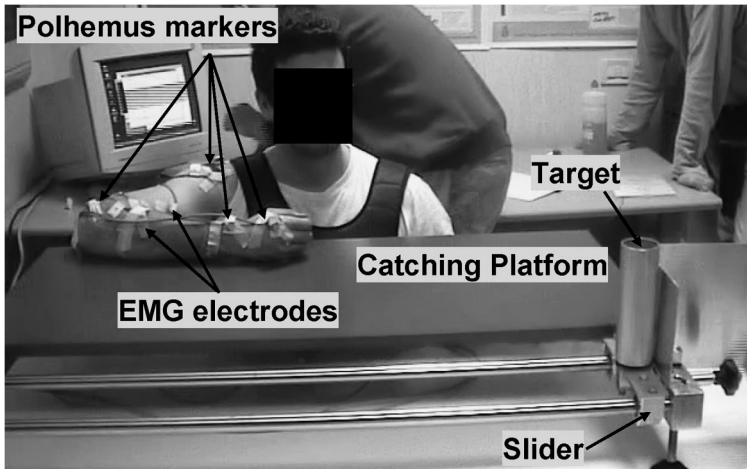


Figure 2. Experimental set-up for motion analysis: the subject is wearing markers while he is catching a moving target on the catching platform.

handle on the object. Arm movement was planar and parallel to the table surface. The subject was not aware of the slider start time and velocity. The trajectories of the markers were acquired and then imported in the biomechanical model described in Section 3.2.

The motion can be considered quite planar so the parameters are relative to the transverse ZX plane. Five catching experimental trials with the same subject and the same maximum slider linear velocity (1.5 m/s) were analyzed. Figure 3 depicts a sketch of the system and the subject posture in the ZX plane.

3.2. Numerical Model

In order to develop a numerical model of the human arm during the execution of the reference task, ADAMS/View software and its plug-in LIFEMOD were exploited. In the first approximation, the human body was considered as a group of rigid bodies connected together through conventional mechanical couplings. The interfaces between the human links, the mechanical device and the environment were modeled with contact ellipsoids and elastic bushing (6 d.o.f. spring–damper elements). The dimensions and the inertial properties of each human link were scaled with respect to weight, height, age, sex and nationality of the subject to be modeled according to the GeBOD (Generator of Body Data) anthropometric database. The number of d.o.f. of each joint was defined according to human anatomy and to the specific problem of the catching task.

The virtual model was placed in a starting posture and an inverse dynamic simulation was performed. The model is driven by motion agents, and all kinematics and dynamics parameters were recorded. Motion agents are virtual markers connected to anatomical repere points by means of 6-d.o.f. spring–damper elements.

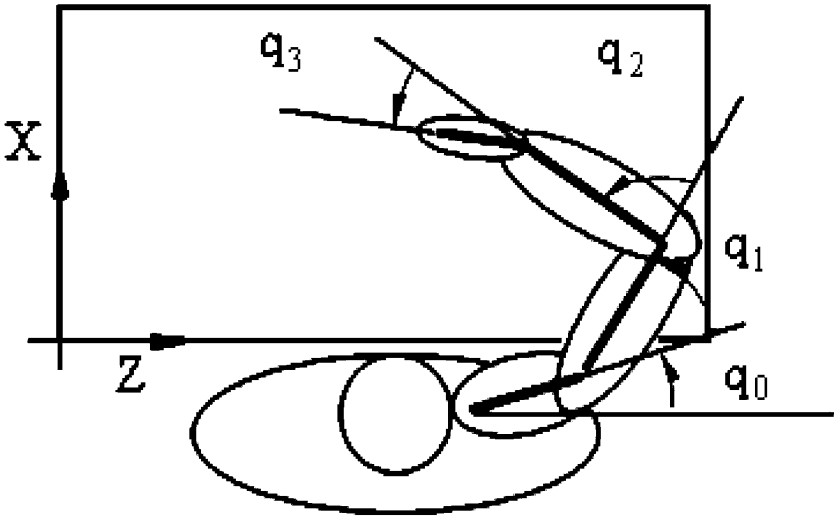


Figure 3. Schematic representation of the human arm and of the joints angles in the plane ZX, where q_0 , q_1 , q_2 and q_3 correspond to the rotation angles of the scapulo-thoracic, shoulder, elbow and wrist joints, respectively.

Each motion agent corresponds to the real marker placed on the real human arm (Fig. 4). The trajectories of the real markers acquired using the motion capture system were converted in ASCII files and finally imported in the modeling software. A forward-dynamics simulation was then performed. The joints were driven using angulations based on the angle history recorded during the previous inverse-dynamic simulation. All the forward-dynamics information was extracted using the ADAMS/PostProcessor. Figure 5 shows the virtual experimental set-up and the human figure in the starting position corresponding to the specific catching task.

3.3. *Stimulation of the Virtual Experimental Set-up and the Human Biomechanical Model*

The main kinematic and dynamic parameters in the catching task are:

- Velocity of the hand along its catching trajectory.
- Angular velocities and angular accelerations of each link.
- Joint torques and joint powers.

The parameters have been calculated on five trials carried out by the involved healthy and trained subject in order to define the maximum kinematics and dynamics parameters of a healthy human arm. The results are presented in Tables 1 and 2, and were used as design specifications of the NEURARM.

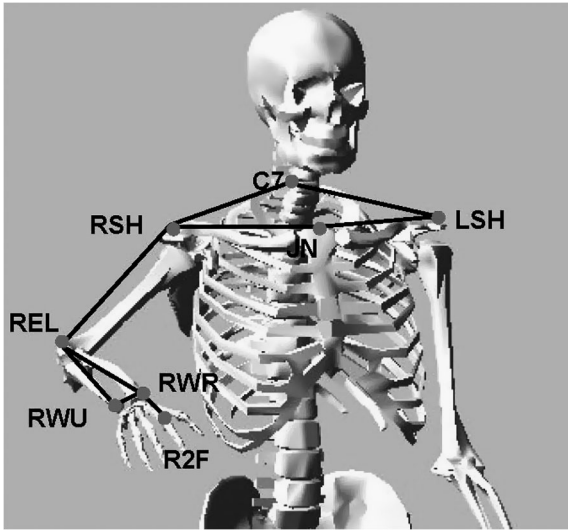


Figure 4. Placement of the Fastrack Polhemus receivers on anatomical landmarks: spinous process of the seventh cervical vertebrae (C7), the jugular notch where the clavicles meet the sternum (CLAV), the left and right acromio-clavicular joint (LSHO, RSHO), the right lateral epicondyle approximating the elbow joint axis (RELB), the right wrist bar thumb side (RWRA), the right wrist bar pinkie side (RWRB), and the dorsum of the right hand below the head of the second metacarpal (RFIN). C7, JN and LSH are acquired in the rest position. The landmark displacements is consistent with one of the protocols of the LIFEMODE plug-in of ADAMS software.

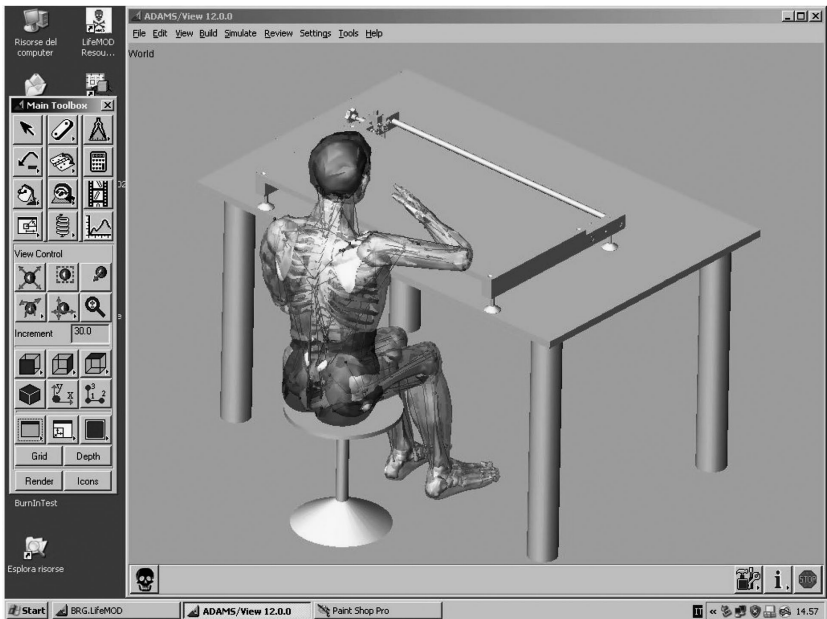


Figure 5. Example of the ADAMS/Postprocessor that was used to simulate the virtual experimental set-up and the human biomechanical model.

Table 1.

Joints angular velocities (\dot{q}) and accelerations (\ddot{q}) of the human arm calculated with the biomechanical model (max and min average values and standard deviations (SD) considering the five experimental trials); the angles origins and directions are indicated in Fig. 3

	Max \dot{q} (SD) (deg/s)	Min \dot{q} (SD) (deg/s)	Max \ddot{q} (SD) (deg/s ²)	Min \ddot{q} (SD) (deg/s ²)
Scapula (q_0)	310 (28)	-11 (13)	3133 (330)	-3495 (421)
Shoulder (q_1)	288 (23)	-6 (4)	2578 (350)	-3392 (483)
Elbow (q_2)	19 (16)	-298 (44)	3664 (1066)	-2078 (244)
Wrist (q_3)	345 (124)	-658 (51)	13765 (3243)	-9903 (1955)

Table 2.

Joints torques (T) and powers (P) of the human arm estimated with the biomechanical model through an inverse dynamic analysis (max and min average values and standard deviations (SD) considering the five experimental trials); the angles origins and directions are indicated in Fig. 3

	Max T (SD) (Nmm)	Min T (SD) (Nmm)	Max P (SD) (W)	Min P (SD) (W)
Scapula (q_0)	10952 (1960)	-17317 (1604)	26 (3)	-75 (5)
Shoulder (q_1)	7014 (1375)	-3357 (1145)	22 (5)	-11 (4)
Elbow (q_2)	1854 (532)	-3561 (433)	11 (1)	-8 (3)
Wrist (q_3)	206 (91)	-582 (149)	5 (2)	-1 (0.8)

4. Design of the NEURARM Platform

The requirements for the mechanical design of the actuation and transmission systems for the NEURARM were obtained from the inertia, torques and power of the human arm.

Table 3 shows the main functional properties of the human arm and the technical solutions selected for the NEURARM.

The NEURARM design is based on the implementation of a lumped parameter model that replicates the main features of the human arm. In addition, the robotic experimental platform allows us to test several configurations of the NEURARM by changing the settings of the system parameters.

4.1. Mechanical Structure

The mechanical design of the platform was designed to meet the following technical requirements derived from the desired functional properties summarized in Table 3:

- Low friction and high reversibility of joints.
- Links size, kinematic and dynamic properties of the NEURARM equivalent to those of the human arm.

Table 3.

Comparison between the human arm and NEURARM functional properties

Human arm	NEURARM
Muscles (non-linear actuators)	Hydraulic pistons in series with non-linear springs
Agonist–antagonist tendon driven	Agonist–antagonist cable driven
Tendons fixed on the bones	Two configurations: cables fixed on the link (forearm) and on the joint (shoulder)
Tunable contraction force	Electrovalves and pressure sensors
Muscle spindles (stretching sensors)	Linear potentiometers on the pistons
Joint receptors (angle sensors)	Angle sensors on the joints
Golgi tendon organs (tension sensors on the tendons)	Load cells on the cables
Sensory hand	Load cell in the end-effector

Table 4.

Dimensional and dynamic parameters comparison

	Human arm	NEURARM
Upper arm		
mass (kg)	2	1.83
COM ratio	0.436	0.421
inertia (kg m ²)	0.0647	0.0644
range of motion (deg)	180 (–40–140)	180
Forearm		
mass (kg)	1.28	0.83
COM ratio	0.509	0.49
inertia (kg m ²)	0.032	0.022
range of motion (deg)	–10–145	0–142

- Workspace equivalent of the human arm range of movement during the execution of planar movements.

The geometrical features of the links were designed to imitate those of a 95 percentile model of a human male defined according to the biomechanical model:

- Upper arm length = 0.332 m.
- Forearm length = 0.278 m.

The desired mass and the inertia of each link are fundamental dynamical parameters. They were extracted from anthropometric parameters [15] related to the mean male weight and height for the European region [13]. Table 4 compares the properties of the human arm and those of the NEURARM.

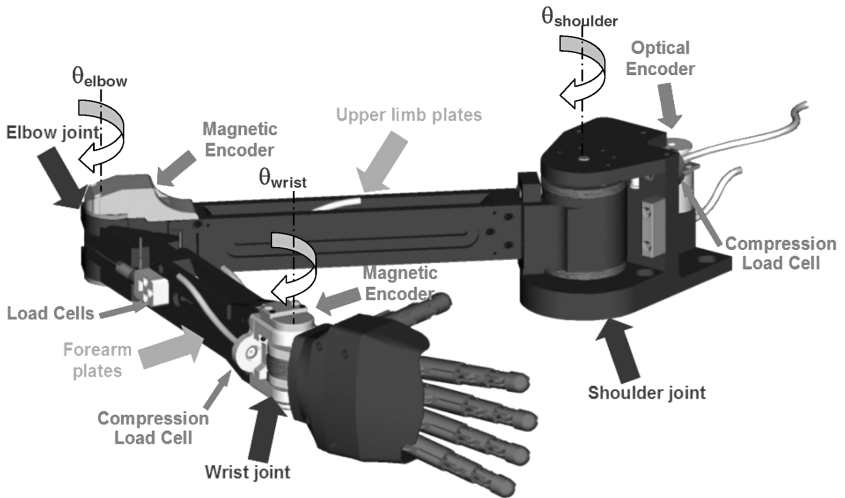


Figure 6. NEURARM planar robot arm: complete configuration.

The implemented kinematic chain is based on a planar robotic arm with two links and two revolute joints with rotation axes perpendicular to the reference plane. The elbow joint corresponds to the actual flexion/extension axis of the human elbow. The rotation axis of the shoulder revolute joint of the NEURARM platform corresponds to the sagittal axis of the gleno-humeral joint. In order to avoid kinematic redundancy, the contribution of the scapula was not implemented. Figure 6 shows the overall mechanical design of the NEURARM prototype.

Aluminum was chosen in order to meet the required weight–dimension ratio. Angular contact bearings in the shoulder and elbow joints were used to provide low friction values and minimum deflection of the links. The current prototype of the NEURARM robotic platform is shown in Fig. 7.

The NEURARM structure was designed in a modular way in order to facilitate the adjustment of the main geometrical and dynamical parameters. The two joints are connected using two couples of parallel plates that provide an appropriate flexional stiffness along the vertical plane. The empty space between the two plates is useful for housing the electrical connections, the sensors and the electronic components. The inter-axes distances between the joints can be easily changed by modifying the plate geometry. A groove that was milled along each plate allows the incorporation of additional masses that can increase the mass and the inertia values of the two links. The masses can be placed in several positions along the links to make it possible to adjust the inertia and center of mass. Figure 8 shows a detailed drawing with the possible location of additional mass. This feature can be used to reproduce the dynamic parameters of the human forearm reported in Table 4. By adding a mass of 0.45 kg, the new dynamic parameters for the forearm are:

- Mass = 1.28 kg.

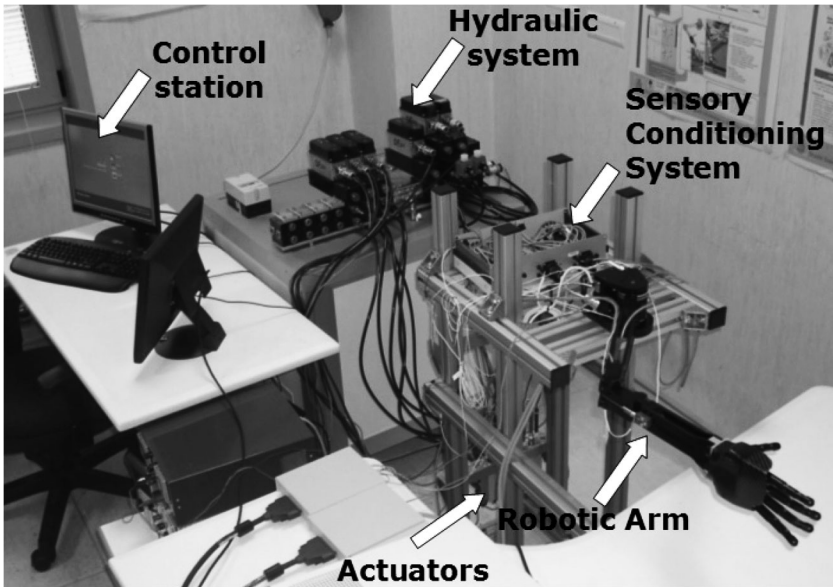


Figure 7. Current prototype of the NEURARM planar robot arm without the wrist joint.

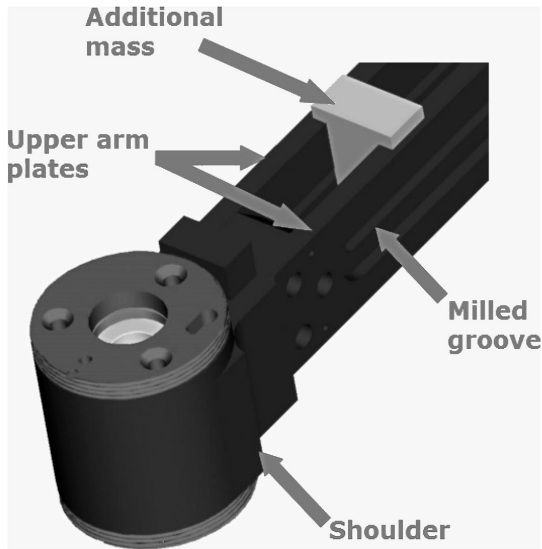


Figure 8. Example of placement of an additional mass to modify the dynamic features of the link.

- COM ratio = 0.503.
- Inertia = 0.032 kg m².

Each joint was provided with mechanical stops to define the work space of the NEURARM. The range of motion of the NEURARM is comparable to the human

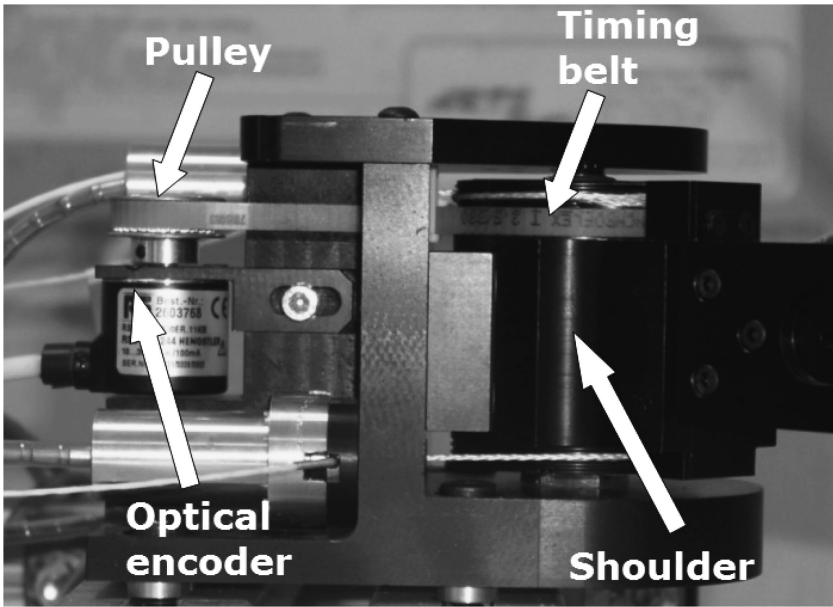


Figure 9. Timing belt and optical encoder on the shoulder joint.

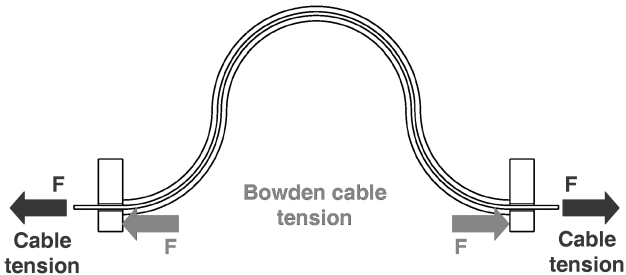


Figure 10. Working principle of the Bowden cables in the static condition: the forces exerted by the endings of the sheaths correspond to those applied on the cables.

arm as reported in Table 4. The work space was measured by means of goniometers integrated in each joint. The shoulder was endowed with a timing belt for amplifying the shoulder rotation angle and for augmenting the angular resolution of the encoder (Fig. 9).

4.2. Transmission system

4.2.1. Cable-driven transmission

The human arm exploits an extrinsic agonist–antagonist actuation scheme for its joints. In order to replicate the human arm features by means of a light-weight structure, a tendon-like transmission based on Bowden cables and remote hydraulic actuators were adopted [36]. The working principle is shown in Fig. 10. The Bow-

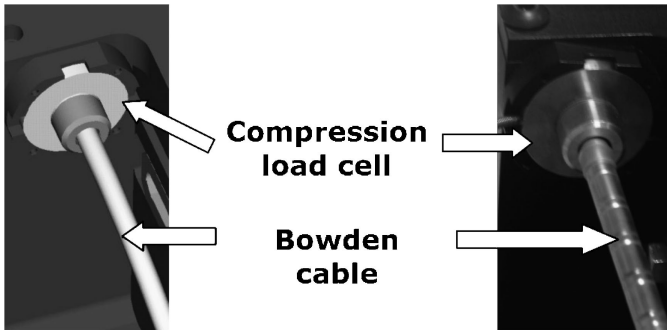


Figure 11. CAD model of the shoulder load cell (left) and its implementation (right).

den cables allow us to reduce the number of mechanisms such as gears, pulleys and belts in the arm, and they transmit the forces directly to the joints.

A new Bowden cable, Nokon Konkavex cable (Nokon, Sussen, Germany), was used to provide high efficiency in force transmission with a lightweight structure. It is composed of a liner made of Teflon reinforced with glass fibers and an aluminum cable housing to provide more precise force transmission than a classical Bowden cable. The assembled transmission is shown in Fig. 11.

The cable is lightweight, high strength, low creep and high flexibility. A trade-off analysis between the standard steel cable and the cable made by other materials was carried out. The Vectran high-performance fibers were selected. By comparing steel and Vectran cables of the same diameter, the main advantages of Vectran cables are seen to be zero creep, lightweight structure and higher bending capacity, with the same maximum strength. Due to the bending capacity it was possible to wrap the cable around shafts and pins of small diameters, reducing the overall size of the transmission and actuation groups.

4.2.2. *Shoulder Joint*

The shoulder joint was based on a classic pulley with two driven antagonistic cables. Two compression load cells were integrated on cables to measure the force exerted by the sheaths (Fig. 11). According to the working principle of the Bowden cables (Fig. 10), these forces correspond to the difference between the tensions on the cables and the friction forces between the cables and the internal liners. This technical solution simplified the measurement of the tensions applied by the cables to the shoulder joint because it avoided the placement of the load cells directly on the pulley where the cables wind and unwind.

4.2.3. *Elbow Joint*

The elbow joint was designed in order to obtain tendon routing that mimics the tendon routing of the human elbow [37]. The cables for the extension and flexion of the elbow were attached on the forearm as the tendons of the triceps and brachialis muscles. During the extension phase, the elbow behaves like a pulley with a constant radius because the extensor cable unwinds on the processed groove. In a different

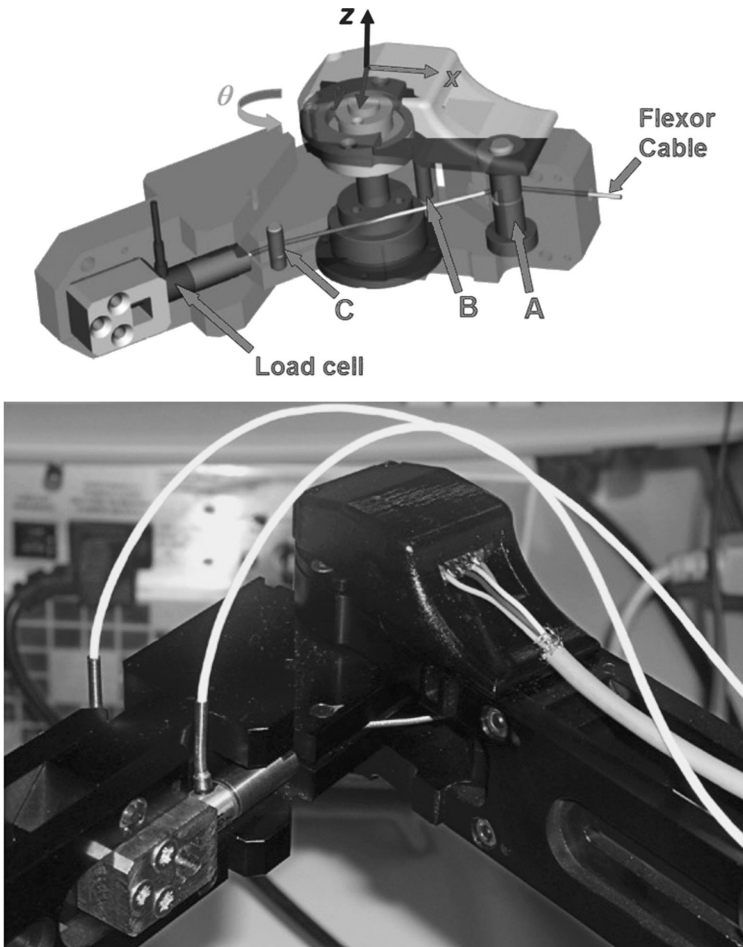


Figure 12. Flexion mechanics of the elbow joint: the cable coming from the upper arm wraps on the rotating shaft A and passes around the pins B and C. The cable extremity has been fixed to the forearm through a load cell. A magnetic absolute encoder has been directly coupled with the elbow rotating shaft and placed on the top of the elbow.

way, the flexor cable passes through the upper arm, around the rotating shaft A and the pin C, and then reaches the forearm (Fig. 12). When the elbow is extended the cable is in contact with a second pin B in a similar way as in the human elbow [11]. Load cells were located at the two cables extremities; they were coupled with the forearm by means of screws. The configuration of the load cells allows the measurement of the net forces applied at the joint by the cables, similar to the Golgi tendon mechanoreceptors in the human arm.

Given the elbow geometry, the flexion motion can be divided in two phases: (i) the cable is stretched by the pin B until a critical flexion angle (Fig. 13) and (ii) the cable is stretched only by the shaft A and the pin C (see Fig. 14). The

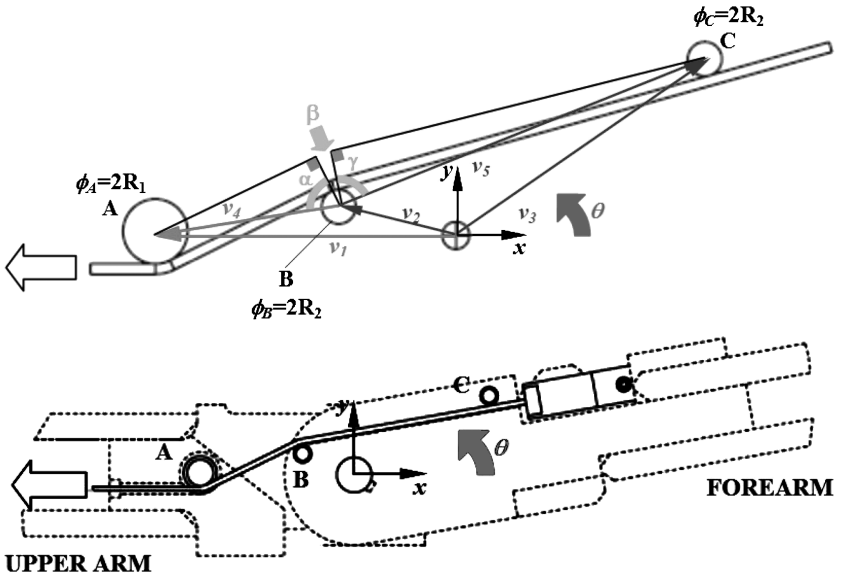


Figure 13. Analytical model (upper) and mechanical sketch (lower) of the elbow cable path wrapping on pin B during phase 1 when the cable is stretched by pin B until a critical flexion angle. The cable unwraps on pin B during the increase of the elbow angle θ .

behavior of the cable during the flexion of the elbow can be described using an analytical model.

Using a reference frame with origin in the elbow center of rotation and x -axis parallel to the upper arm, the vectors \bar{v}_1, \bar{v}_2 and \bar{v}_3 that identify the center of elements A, B and C are defined (Fig. 13). Also the values of radius for shaft (R_1) and pins (R_2) are defined. Vectors measuring distance and orientation between the centers of the shaft A and the pin B, and the centers of the pin B and the pin C are written in vector form as follows:

$$\begin{aligned} \bar{v}_4 &= \bar{v}_1 - \bar{v}_2 \\ \bar{v}_5 &= \bar{v}_3 - \bar{v}_2. \end{aligned} \tag{1}$$

As shown in Fig. 13, during the first flexion phase, the modules of \bar{v}_2 and \bar{v}_3 are constant. The triangle $(\bar{v}_2, \bar{v}_3, \bar{v}_5)$ rotates with the forearm of the same angle θ . The rotation matrix R is defined as:

$$R = \begin{bmatrix} \cos \vartheta & -\sin \vartheta \\ \sin \vartheta & \cos \vartheta \end{bmatrix}, \tag{2}$$

where θ is the elbow rotation angle. New vector positions $\bar{v}_{2R}, \bar{v}_{3R}, \bar{v}_{4R}$ and \bar{v}_{5R} are computed as follows:

$$\begin{aligned} \bar{v}_{2R} &= R\bar{v}_2 \\ \bar{v}_{3R} &= R\bar{v}_3 \end{aligned} \tag{3}$$

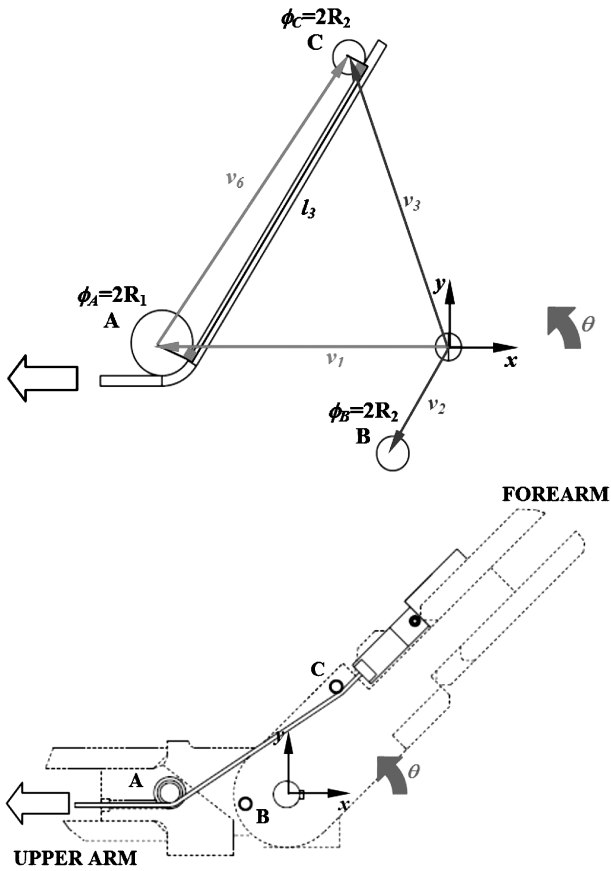


Figure 14. Analytical model (upper) and mechanical sketch (lower) of the elbow cable path wrapping on pin C and shaft A during phase 2. As the human tendon, the cable is stretched between the shaft A (rotating) and the pin C.

$$\bar{v}_{4R} = \bar{v}_1 - \bar{v}_{2R}$$

$$\bar{v}_{5R} = \bar{v}_{3R} - \bar{v}_{2R}.$$

The condition of cable detachment from pin B is obtained when the β angle is null (Fig. 13). The estimation of β has been achieved using some geometrical considerations about the wrap condition of the cable on elements A, B and C. Considering that the cable is tangential to the pins A, B and to the pins B, C, two right triangles can be constructed on the vectors \bar{v}_4 and \bar{v}_5 . The cathetus magnitude of the first triangle is the sum of R_1 and R_2 , whereas in the second triangle it is two times the length of R_2 . The resulting α , γ and β angles can be computed as follows:

$$\alpha = \arccos \frac{R_1 + R_2}{\|\bar{v}_{4R}\|}$$

$$\gamma = \arccos \frac{2R_2}{\|\bar{v}_{5R}\|} \quad (4)$$

$$\beta = [\arg(\bar{v}_{4R}) - \arg(\bar{v}_{5R})] - (\alpha + \gamma),$$

for $\beta = 0$:

$$[\arg(\bar{v}_{4R}) - \arg(\bar{v}_{5R})] - (\alpha + \gamma) = 0. \quad (5)$$

By considering (3) and (4), the following critical angle for the cable detachment has been computed: $\theta_c = 0.358$ rad. When $\theta = \theta_c$, the first phase of flexion kinematic ends.

When $\theta > \theta_c$, the second flexion phase starts and the cable is strength between A and C (Fig. 14). The vector \bar{v}_6 is defined as:

$$\bar{v}_6 = \bar{v}_1 - \bar{v}_{3R}. \quad (6)$$

Starting from the same observation on the right triangles used in the first flexion phase, the cable length between the two tangent points can be computed as:

$$l = \sqrt{\|\bar{v}_{6R}\|^2 - (R_2 - R_1)^2}. \quad (7)$$

The complete analytical model of the elbow in terms of geometry elements and wrapping angles was expressed as a function of the θ angle; therefore, an analytical correlation between cable movements and elbow angles was calculated (Fig. 15).

As demonstrated above, the elbow behavior depends on the θ angle and the critical angle θ_c identifies two flexion phases. The moment arm of the force applied by the flexion cable of the elbow depends on the elbow configuration (Fig. 16). In the

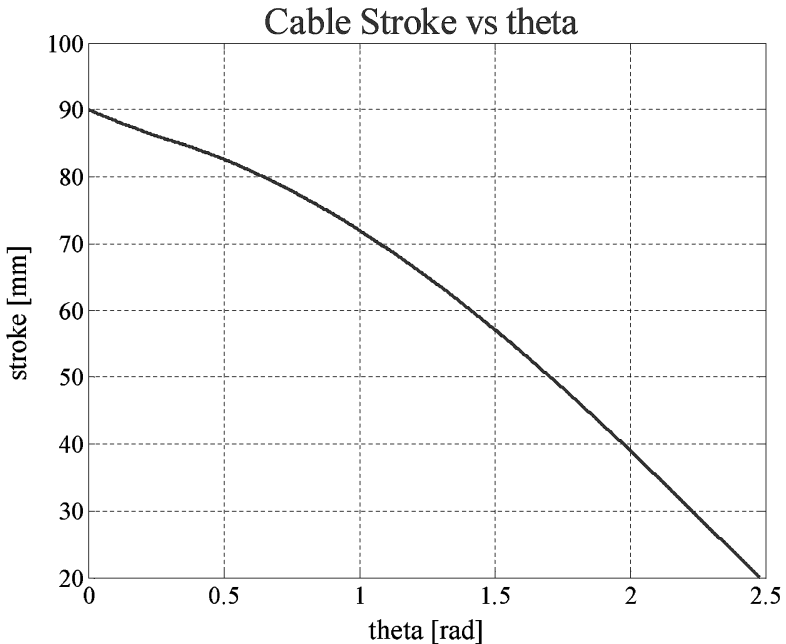


Figure 15. Relationship between the stroke of the flexor cable and the elbow angle.

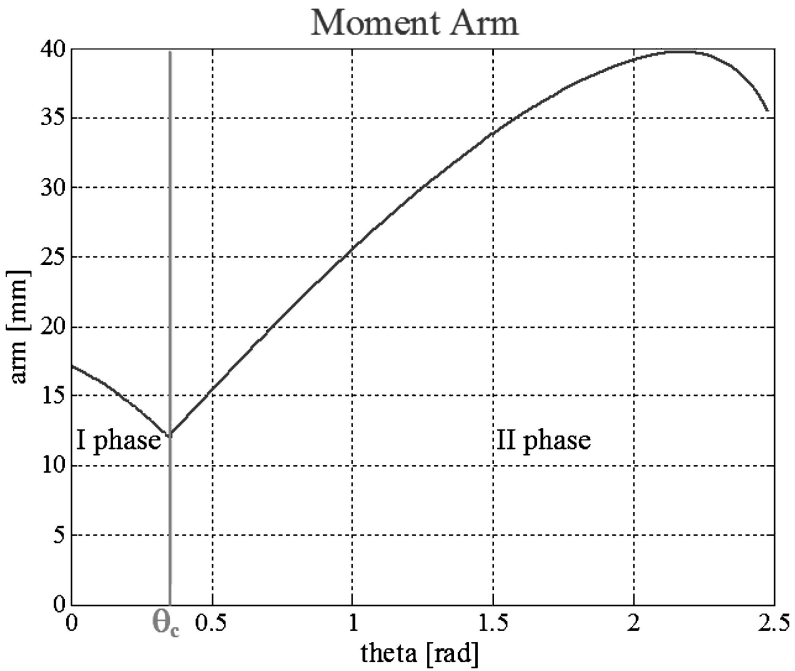


Figure 16. Moment arm of the elbow during the flexion movement depends on the θ angle and on the flexion phases.

first phase the moment arm decreases because of the rotation of the pin B that moves the cable closer to the rotation center of the elbow. When the cable is detached from B (second phase), the moment arm increases because the cable wraps around the shaft A, so its distance from the center of rotation increases. The maximum value of the moment arm is obtained when the cable is parallel to the y -axis. Finally, the moment arm decreases again because the cable again moves closer to the rotation center until the mechanical stop is reached.

4.3. Actuation System

The desired target task is demanding for the actuation system because the required torque and power values are relatively high, and for that reason we decided to adopt hydraulic actuators. The hydraulic cylinder is a linear actuator and can apply a large force in short time as requested in high-speed catching tasks. In addition, the power of hydraulic actuators is such that they are able to lift and hold heavy loads without brakes, and move heavy objects even at slow speeds. A hydraulic system can be controlled with high precision obtaining high-resolution positioning of the rod of the cylinder [38]. Finally, hydraulic actuation is able to provide a high value of power/weight ratio allowing us to reduce the overall size of the actuators system. The NEURARM position control of the actuation system has a bandwidth of about 3 Hz (-3 dB). The friction model is not considered because four load cells are used

to measure the cable tension at the end of the cables (see Section 4.4.1) so the bio-inspired controller that is under development will exploit the sensors information.

4.3.1. Hydraulic Power Pack

The specific hydraulic system selected for this application is shown in Fig. 17. The hydraulic power pack consists of a gear pump connected with a three-phase AC electric motor (1.1 kW, 1390 rpm), a 30-l oil tank, an accumulator (250 bar, 5.7 l) and modular plates in order to connect up to 10 directional control valves for the pistons. An unloading valve (350 bar, 40 l/min) is placed on the hydraulic circuit for safety against over-pressure. By using accumulators to store energy, the hydraulic power unit only needs to provide slightly more than the average demand, increasing

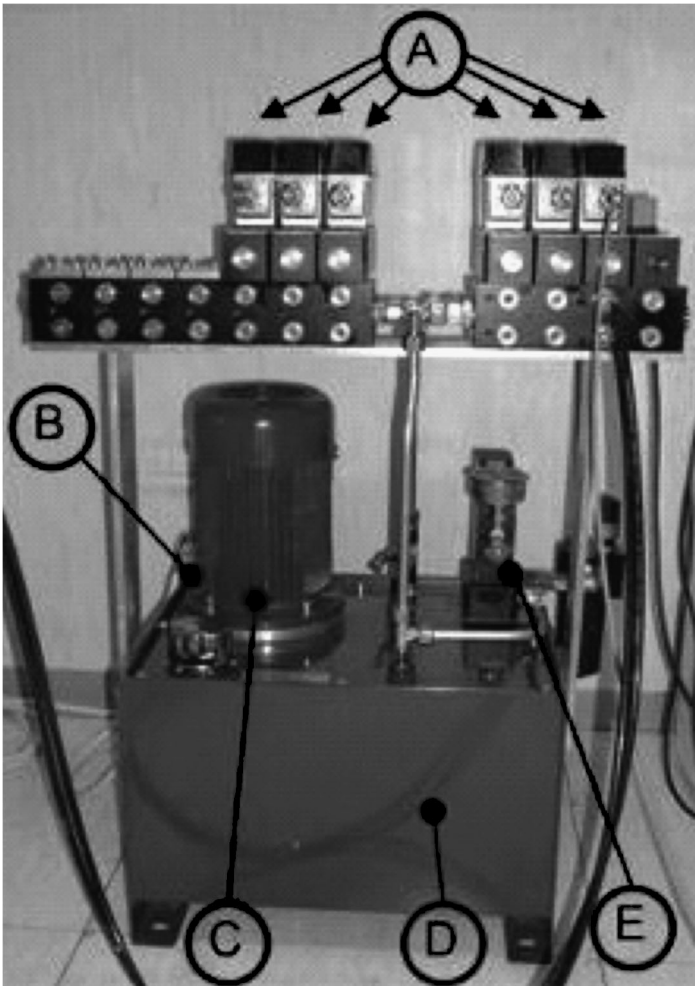


Figure 17. Hydraulic system: (A) electro-valves, (B) accumulator, (C) motor, (D) oil tank and (E) unloading.

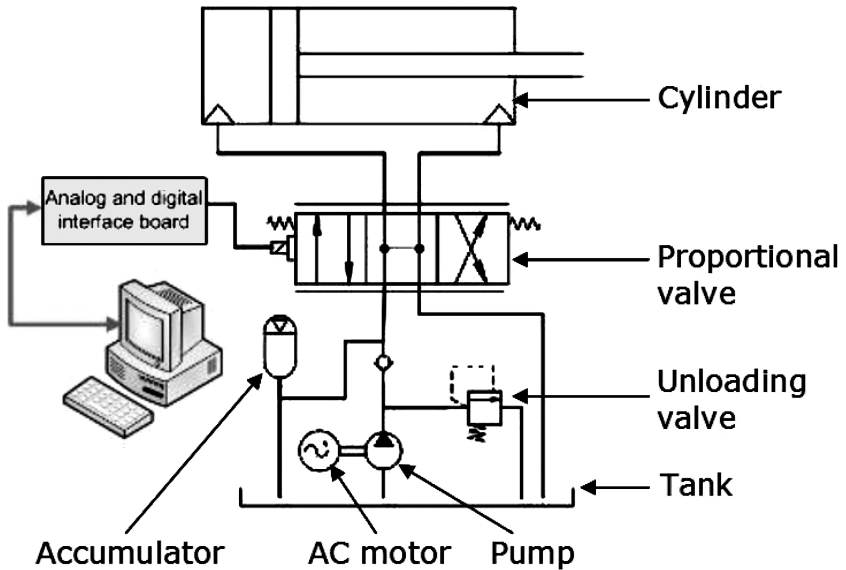


Figure 18. Scheme of the hydraulic actuator.

efficiencies for machines with varying load cycles and the time response of the system. The hydraulic power pack was provided with six direct-operated proportional DC valves, series D1FP*S (Parker Hannifin, and six single-rod double-acting hydraulic cylinders CHL (Parker Hannifin, Elyria, OH, USA) with a stroke of 50 mm and a maximum operating pressure of 100 bar. The scheme of the hydraulic circuit for one cylinder is shown in Fig. 18.

Each electro-valve is a three-land-four-way valve with an overlapped spooltype. Using a tension control signal (± 10 V), acting on the spool position by means of a PID controller embedded on the valve electronic board, the velocity of the piston movements is controlled in a linear way. Positive input voltages sent to the electro-valve cause the oil flowing from the pump to the first chamber of the cylinder determining the withdrawl of the cylinder rod. Negative voltages cause the rod to come out.

The spool valve has a step response of 3.5 ms and a frequency response of 350 Hz (-3 dB) with an input signal of $\pm 5\%$ of the maximum value of the control signal. Compact size and light weight are the main advantages of the CHL cylinder compared to a standard manufacturing hydraulic cylinder. The cylinder body is aluminum and the piston is provided with low-friction Teflon/bronze seals in order to reduce the stiction value and to increase the dynamic performance of the cylinder. The diameters of the pipes connecting the proportional valves and the cylinders have been calculated to provide full recharge of the oil contained in the cylinder chambers during operation for avoiding gas inclusions that can cause non-linear behavior of the actuators.

4.3.2. Actuator Configuration

The NEURARM actuation system was provided with four CHL cylinders mounted on an aluminum bar and fixed by screws. Another aluminum bar was placed above the cylinders as a reference frame for the endings of the Bowden cables (see Fig. 19). Each cable coming out from the bar is connected to the rod extremity of the cylinder by means of a stay rod. This solution enables simple and fast adjustment of the cable preload. The rod extremity was also provided with a clamp for the linear potentiometer used for measuring the piston stroke.

4.3.3. Non-linear Spring

In order to implement joint torque and stiffness control, a non-linear spring element to be mounted in series with each actuator was designed. A first solution is obtained using Belleville washer springs with different stiffness values, stacked one on top of each another (Fig. 20). The stack procedure was optimized in order to ob-

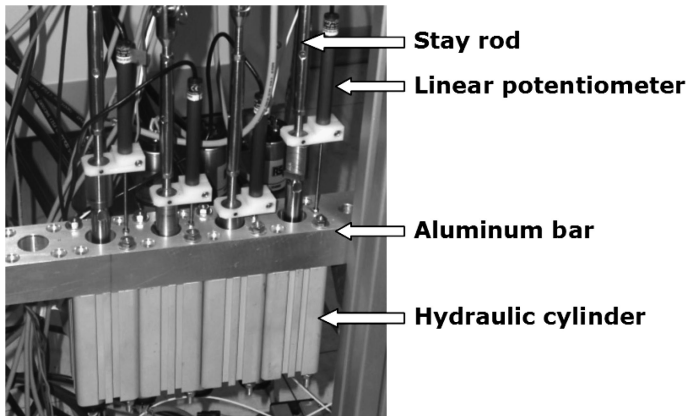


Figure 19. Actuator configuration is composed of four linear hydraulic cylinders mounted on an aluminum bar and connected to the cables by means of stay rods; four linear potentiometers are used to measure the displacements of the cylinder rod extremities.



Figure 20. CAD model (left), and disassembled (middle) and assembled (right) first prototype of the non-linear spring that works in compression and that will be connected in series with the actuator.

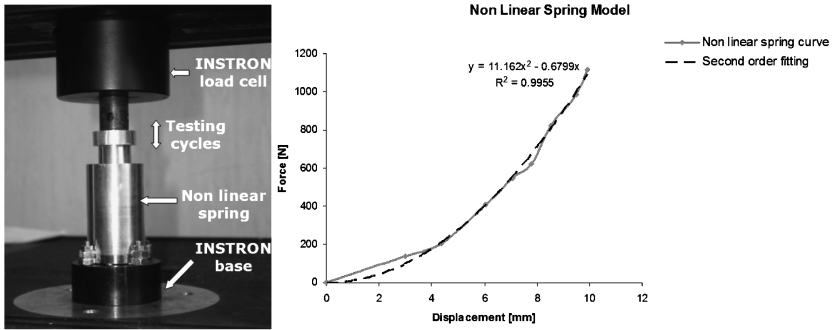


Figure 21. Experimental set-up for the characterization of the non-linear spring (left) and the characteristic curve (right).

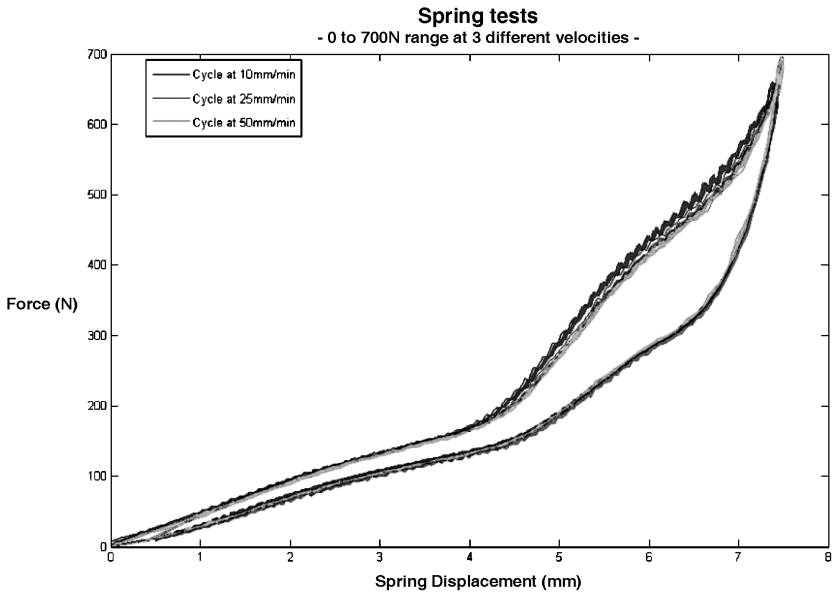


Figure 22. Experimental data fitting using the ninth polynomial function. The spring shows high repeatability and independency of hysteresis from the loading and unloading velocity.

tain a second-order-like behavior. The first prototype was characterized under the INSTRON Series 4400 testing system as shown in Fig. 21.

The spring was tested by means of a repeated load/unload cycle from 0 to 700 N in order to evaluate the characteristic curve, the repeatability and the hysteresis. The force-length curve depicted in Fig. 22 shows hysteresis in the spring probably due to the friction and stick-slip effects between the stacked washers. In addition, the load and unload curve is too segmented, showing different slopes corresponding to the different stiffnesses of the stacked up springs. In order to decrease the hysteresis a proposed solution is to fill the system with lubricant oil. By adding lubricant oil it is possible to reduce the friction effects, as well as to decrease the segmentation of

the curve. A different solution is through design and development in order to obtain a characteristic curve closer to a second-order curve.

4.4. Sensory System

4.4.1. Tension Sensors on the Cables

The shoulder and the elbow joints were equipped with four load cells (series XFL225D and XFTC301; FGP Sensors, Paris, France), two for each joint. Two configurations were implemented for testing different technical solutions: (i) the direct measurement of cable tensions acting on the elbow by using load cells in series with the two cables (already described in Section 4.2.3 and (ii) the indirect measurement of the two tensions acting on the shoulder by measuring the forces exerted by the two Bowden cables.

Load cells sensitive to compression have been used in the second configuration, and two specific components for fixing the normal force components were fabricated and integrated (Fig. 23). The load cells were placed at the connection points between the sheath and the structure of the joints so that they measure the forces acting on the joints and exerted by the two pistons.

4.4.2. Angle Sensors

A rotational optical relative encoder (1024 pulses per revolution) was used to measure the shoulder angular position. A new absolute angular displacement sensor, designed around the Honeywell HMC1512 MR sensor, was developed to obtain accurate measurements of the elbow angular position. The absolute 180° angular measurement, the 0.05° resolution, and the reduced sensitivity to shocks and vibrations allowed an accurate estimation of the elbow angular displacement, compared to a traditional relative encoder-based solution.

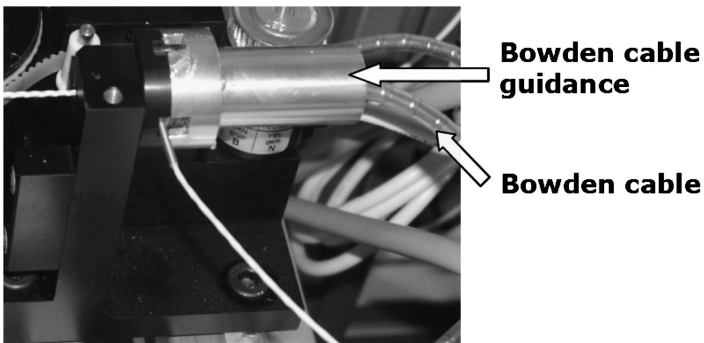


Figure 23. Bowden cable guidance used for fixing the final part of the Bowden cables acting on the shoulder, and for guaranteeing the reliability and repeatability of the normal component of the forces measured by the two compression load cells.

4.4.3. Potentiometers on the Pistons and Pressure Sensors

The pistons were equipped with linear potentiometers SLS095 (LEANE) that measure the displacement of the rods. Moreover, each piston was equipped with one pressure sensor for each chamber of the cylinder.

4.4.4. Load Cell in the End Effector

A two-dimensional load cell (F_x and F_y components, 1000 N maximum load on each channel) has been integrated into the end-effector of the arm to measure the catching force between the arm and the environment.

4.5. Hardware and Software Integration

A dedicated electronic unit was developed to meet the requirements for power and signal conditioning, and to connect to the DAQ board inputs (± 10 V for analog signals and 5 V TTL for digital) (see Fig. 24). The system is able to accept up to eight analog signals for each joint (two from the load cells, four from the pressure sensors and two general purpose analog inputs for future use), one digital input from an encoder (both A and B channels are converted in pulse and direction for proper connection to DAQ board counters), and up to eight Hall effect digital limit switches for piston stroke. Also analog outputs from DAQ boards need to be buffered because the current necessary for the hydraulic system exceeds DAQ electrical specifications. To prevent electrical noise during analog signal acquisition all systems were shielded by housing the circuit boards in a shielded metal box and cabling sensors with shielded cables.

The NEURARM control algorithms run on a National Instruments PXI, configured with a real-time embedded controller (PXI -8196 RT) with a 2.0-GHz Pentium M 760, and two National Instruments Data acquisition cards (DAQ 6071E and DAQ 6713E) are used to acquire the analog input and to drive the electro-valves as shown in Fig. 25. The PXI stand-alone controller runs a real-time operating system capable

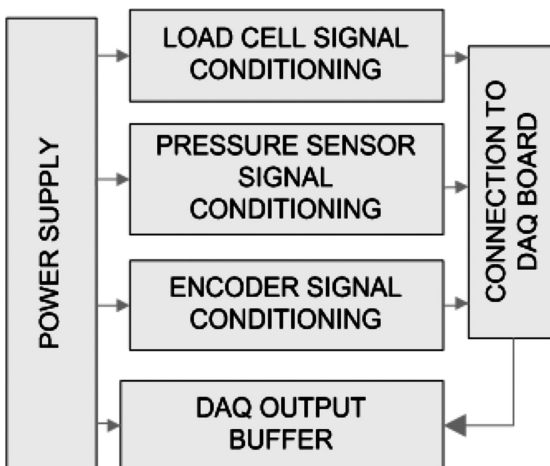


Figure 24. Sensor conditioning system (SCS).

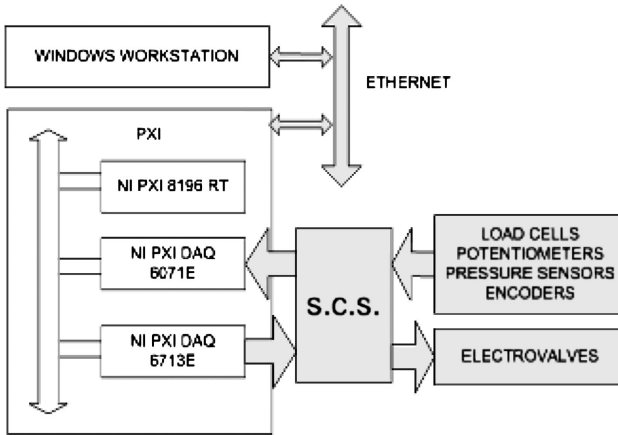


Figure 25. Software architecture.

of 57-kHz single-channel PID loop and is connected through an Ethernet bus to a PC running Windows XP. The control algorithm, developed using the Labview Real Time module, has to be compiled first on the remote PC and then to be downloaded to the PXI, where it is executed. The PC runs non-real-time tasks from the control panel, and permits watching of the current variables state and the on-line changing of the control loop parameters.

5. Experimental Results and Discussion

The planar catching movement performed by the human subject was replicated by implementing a force controller in order to validate the design approach and the kinematics performance of the NEURARM. In particular, the fourth subject trial was characterized by a time to impact of 0.5 s and was selected as a benchmarking task for the NEURARM. The catching trajectory was modeled as a straight line interpolating the experimental hand markers trajectories acquired as described in Section 3. The velocity of the center of gravity of the human hand along its trajectory was calculated by the biomechanical model and was modeled using a fourth-order polynomial law and it was considered as the desired trajectory for the NEURARM end-effector. The reference trajectories for the joint angles were calculated through an inverse kinematics analysis. The NEURARM was analyzed as a two-link robotic arm, neglecting the contribution of the human scapula and fixing the wrist with respect to the forearm. The sampling frequency used for the experiments was 200 Hz.

Figures 26 and 27 depict the performance of the system in replicating the catching task. The obtained data demonstrated that the NEURARM elbow and shoulder joints are able to track the human joint trajectories.

The profiles of the joint angular velocities are shown in Figs 28 and 29. The angular velocity of the shoulder is lower than the reference one, while the angu-

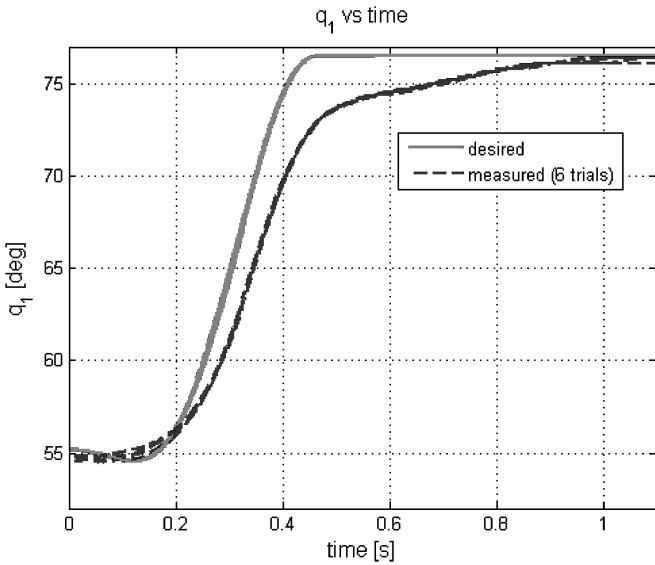


Figure 26. Shoulder angle q_1 during catching task.

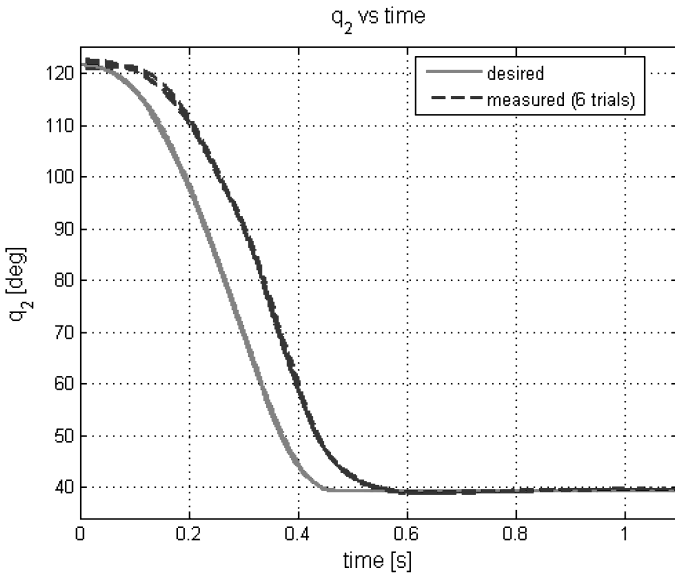


Figure 27. Elbow angle q_2 during catching task.

lar elbow velocity is larger than the reference one. There is a sort of compensation between the shoulder and elbow in order to obtain the required timing of the task. Small deviations in path tracking (both in joint angle and velocity profiles) can be considered to be on account of time delays in the hardware set-up. The implemen-

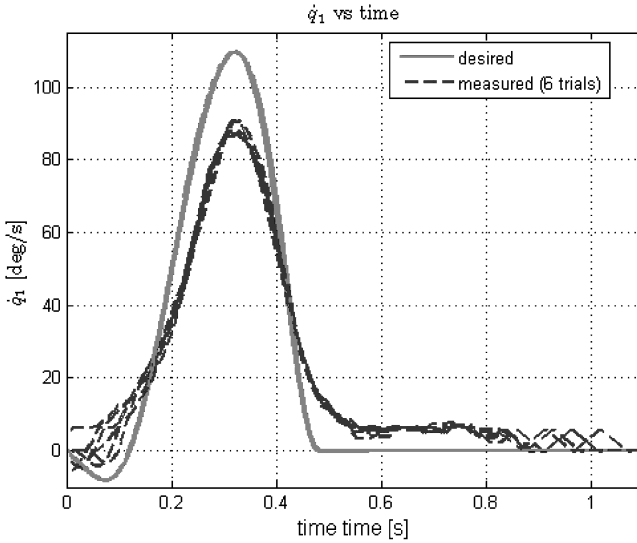


Figure 28. Shoulder angular velocity.

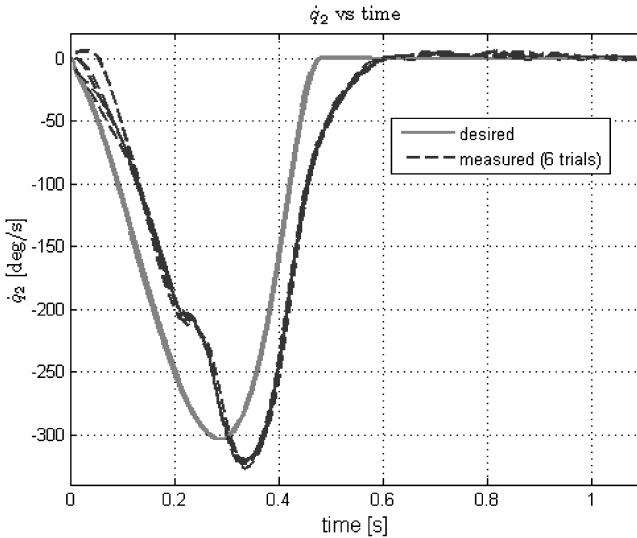


Figure 29. Elbow angular velocity.

tation of a bio-inspired controller is currently ongoing in order to decrease the delay and the oscillations at low speed.

The velocity of the end-effector along the trajectory graph of NEURARM compared with the human one shows the ability of the robotic platform to execute the reference task. The desired, measured and modeled velocities of the end-effector along the trajectories are shown in Fig. 30.

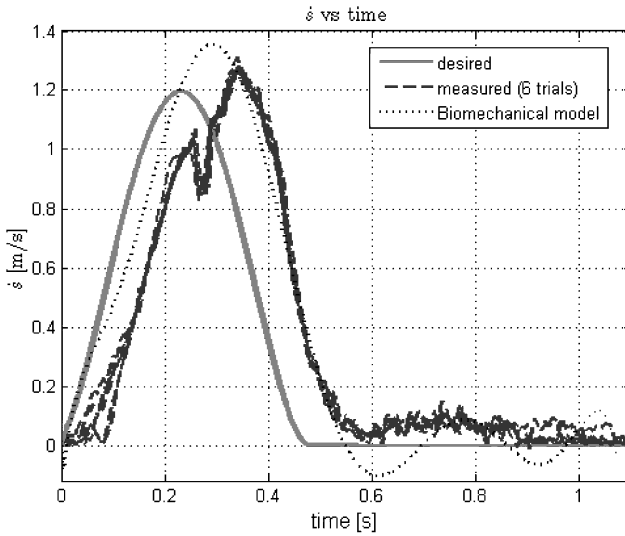


Figure 30. Velocity along the trajectory.

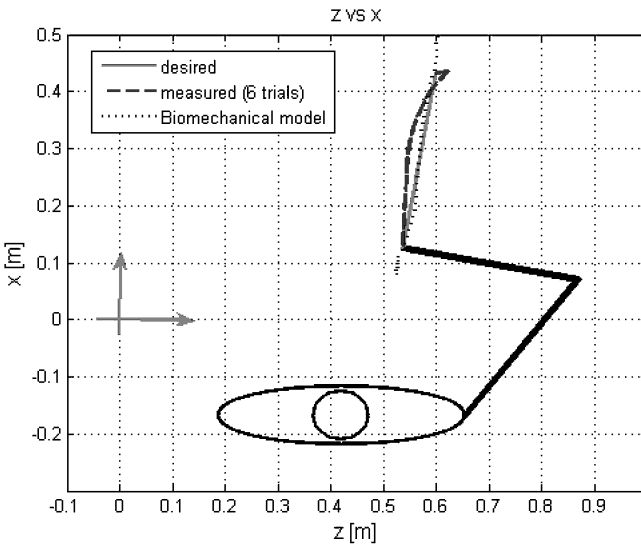


Figure 31. Trajectories of the end-effector in the Cartesian space.

Figure 31 depicts the desired trajectory of the end-effector, the measured trajectory during six different trials and the trajectory of the center of gravity of the human hand in the same task.

The robotic platform shows a good repeatability with low standard deviations and it can be considered reliable to perform neuroscientific experiments. The catching tests were repeated 6 times applying the same reference laws. Figures 26–30 show

Table 5.

Some parameters to show the repeatability of the system

Variable	Mean	Standard deviation	Percentile variation (%)
Max ($ dq_1 $) (deg/s)	88.29	1.78	2.01
Max ($ dq_2 $) (deg/s)	323.14	2.56	0.79
Max ($ dz $) (m/s)	0.54	1.18e-2	2.17
Max ($ dx $) (m/s)	1.19	1.08e-2	0.89
RMSE ($q_{1d} - q_1$) (deg)	1.44	1.68e-2	1.16
RMSE ($q_{2d} - q_2$) (deg)	5.67	0.13	2.28
RMSE ($z_d - z$) (m)	1.23e-2	2.52e-4	2.04
RMSE ($x_d - x$) (m)	2.24e-2	5.98e-4	2.66

graphically the good performance of the system in terms of repeatability. Table 5 summarizes the statistical parameters related to the NEURARM repeatability.

6. Conclusions

This paper presents the biomechatronic design of an anthropomorphic robotic platform aimed at reproducing the behavior of the human arm during some predefined tasks. It will be used for the implementation and assessment of neuroscience models dedicated to the investigation of the unconscious control mechanism of the upper limb.

The human arm is a complex machine and it is hard to replicate in all its characteristics. The design approach presented takes into account only those properties that are considered important for the achievement of the goal according to neuroscientists' requirements. The biological structure of the arm is not reproduced, but the functional behavior is experimentally demonstrated to be reproduced by the NEURARM.

The design approach starts with the modeling of the human arm during the task considered. This model can be analytical and/or numerical, and is based on a heavy hypothesis on the human body that must be verified and validated with the experimental results. The outputs of this model are qualitative human arm kinematic and dynamic parameters on which the dimensioning of the mechanical structure and the choice of the actuation system were based. The standard anthropometric dimensions of the human arm, joints torques and powers calculated are the engineering requirements for the biomechatronic design of the robotic arm, and represent the translation into technical meaning of the neuroscientist functional requirements. This design process was applied for the development of the NEURARM platform. It is composed of an anthropomorphic robotic arm moved by tendon-like actuation by means of a Bowden cable transmission system. The actuation is configured with an agonist–antagonist scheme. Hydraulic cylinders with a hydraulic power pack provide the force required by the system to perform the reference task. The platform

is equipped with a sensory system that replicates the functionalities of the human arm. The approach was validated by performing some experiments. Neuroscientists identified the planar catching task as the benchmark experiment to evaluate and compare the performance of the human arm and the robotic one. The NEURARM platform shows high repeatability, and the preliminary catching tests showed good agreement between the kinematical parameters of the NEURARM and the human arm (i.e., joints angular trajectories and velocity, and end-effector velocity along trajectory). The available data demonstrate that the design is appropriate and that real experimental work with neuroscientists can start.

Therefore, NEURARM can be considered a high-performance platform for neuroscience experiments and the design approach can be applied and generalized to other biomechanics artificial machines for neuro-robotics applications.

Ongoing activities are focused on the implementation and testing of model-based torque controllers, incorporating the dynamics of the system (transmission and robotic arm) that will be applied in the future to reduce the system delay in the catching task. In addition, the NEURARM is used to investigate the human model of sensorimotor integration during the learning of reaching tasks. The wrist joint is under manufacturing in order to complete the kinematic configuration of the NEURARM platform. Stroke amplifiers for the hydraulic cylinders have been designed and fabricated in order to cover all the range of motion for each joint and to allow the use of the non-linear spring. The robotic arm will be completed by an integrated and advanced mechatronic hand that will allow the investigation of grasping and manipulation tasks. A new non-linear spring was used to obtain a characteristic force–displacement curve closer to a second-order behavior and will be integrated in the system. Neuroscience experiments will be done using the non-linear springs and the equilibrium point theory in order to investigate the sensorimotor control strategies used by humans and to apply it in the robotic field.

Acknowledgements

This work was supported by the Integrated Project NEUROBOTICS (The fusion of NEUROscience and roBOTICS) (FP6-EU-IST-FET-2003 contract 001917). The authors would like to thank Clemens Eder, Pietro Cirone, Matjis Vermeulen and Gabriel Bismut for their support during the platform assembling and testing, and Nicodemo Funaro, Gabriele Favati, Andrea and Vinicio Alpigiani (Micromecc srl, Pisa), for their support in the fabrication of the mechanical components of the NEURARM.

References

1. A. Berthoz, *Multisensory Control of Movement*. Oxford University Press, Oxford (1993).
2. F. Laquaniti and C. Maioli, The role of preparation in tuning anticipatory and reflex responses during catching, *J. Neurosci.* **9**, 134–148 (1989).
3. B. Hannaford, J. M. Winters, C. P. Chou and P. H. Marbot, The anthroform biorobotic arm: a system for the study of spinal circuits, *Ann. Biomed. Eng.* **23**, 399–408 (1995).

4. L. Zollo, B. Siciliano, C. Laschi, G. Teti and P. Dario, An experimental study on compliance control for a redundant personal robot arm, *Robotics Autonomous Syst.* **44**, 101–129 (2003).
5. L. Zollo, B. Siciliano, E. Guglielmelli and P. Dario, A bio-inspired approach for regulating viscoelastic properties of a robot arm, in: *Proc. IEEE Int. Conf. on Robotics and Automation*, Taipei, pp. 3576–3581 (2003).
6. L. Zollo, E. Guglielmelli, G. Teti, C. Laschi, S. Eskiizmirli, F. Carenzi, P. Bendahan, P. Gorce, A. M. Maier, Y. Burnod and P. Dario, A bio-inspired neuro-controller for an anthropomorphic head-arm robotic system, in: *Proc. IEEE Inter. Conf. on Robotics and Automation*, pp. 12–17, Barcelona (2005).
7. G. Hirzinger, N. Sporer, M. Schedl, J. Butterfa and M. Grebenstein, Torque-controlled lightweight arms and articulated hands: do we reach technological limits now?, *Int. J. Robotics Res.* **23**, 331–340 (2004).
8. W. Townsend, The effect of transmission design on force-controlled manipulator performance, *PhD Thesis*, Boston, MA (1988).
9. K. Salisbury, W. Townsend, B. Eberman and D. Di Pietro, Preliminary design of a whole-arm manipulation system (WAMS), in: *Proc. IEEE Int. Conf. on Robotics and Automation*, PA, vol. 1, pp. 254–260, Philadelphia (1988).
10. B. M. Hove and J. J. E. Slotine, Experiments in robotic catching, in: *Proc. Am. Control Conf.*, vol. 1, pp. 380–385, Boston, MA (1991).
11. A. Kapandji, *The Physiology of the Joints — Upper Limb*. Churchill Livingstone, Edinburgh (1982).
12. J. McIntyre, M. Zago, A. Berthoz and F. Lacquaniti, Does the brain model Newton's laws?, *Nat. Neurosci.* **4**, 693–694 (2001).
13. L. Peebles and B. Norris, *Adultdata: The Handbook of Adult Anthropometric and Strength Measurements: Data for Design Safety*. Department of Trade and Industry, Government Consumer Safety Research, London (1998).
14. D. A. Winter, *Biomechanics and Motor Control of Human Movement*. Wiley, New York (1990).
15. J. M. Winters and S. Woo, *Multiple Muscle Systems: Biomechanics and Movement Organization*. Springer, New York (1990).
16. P. M. McGinnis, *Biomechanics of Sport and Exercise*. Human Kinetics, Leeds (1999).
17. F. E. Zajac, Muscle and tendon: properties, models, scaling, and application to biomechanics and motor control, *CRC Crit. Rev. Biomed. Eng.* **17**, 359–411 (1989).
18. P. A. Huijing, Muscle, the motor of movement: properties in function, experiment and modelling, *J. Electromyogr. Kinesiol.* **8**, 61–77 (1998).
19. N. Hogan, The mechanics of multi-joint posture and movement control, *Biol. Cybernet.* **52**, 315–331 (1985).
20. F. E. Zajac and M. E. Gordon, Determining muscle's force and action in multi-articular movement, *Exerc. Sport Sci. Rev.* **17**, 87–230 (1989).
21. J. McIntyre, F. A. Mussa-Ivaldi and E. Bizzi, The control of stable postures in the multijoint arm, *Exp. Brain Res.* **110**, 248–264 (1996).
22. S. H. Brown and J. D. Cooke, Movement-related phasic muscle activation. I. Relations with temporal profile of movement, *J. Neurophysiol.* **63**, 455–464 (1990).
23. R. D. Keynes and D. J. Aidley, *Nerve and Muscle*. Cambridge University Press, Cambridge (2001).
24. J. V. Basmajian and C. J. De Luca, *Muscles Alive*, 5th edn. Williams & Wilkins, Baltimore, MD (1985).
25. N. Hogan and C. G. Atkeson, Planning and execution of multi joints movements, *Can. J. Physiol. Pharmacol.* **66**, 508–517 (1988).

26. B. B. Edin and A. B. Vallbo, Dynamic response of human muscle spindle afferents to stretch, *J. Neurophysiol.* **63**, 1297–1306 (1990).
27. B. B. Edin, Finger joint movement sensitivity of non-cutaneous mechanoreceptor afferents in the human radial nerve, *Exp. Brain Res.* **82**, 417–422 (1990).
28. B. B. Edin, Cutaneous afferents provide information about knee joint movements in humans, *J. Physiol.* **531**, 289–297 (2001).
29. R. S. Johansson, Tactile sensibility in the human hand: receptive field characteristics of mechanoreceptive units in the glabrous skin area, *J. Physiol.* **281**, 101–125 (1978).
30. R. S. Johansson and G. Westling, Signals in tactile afferents from the fingers eliciting adaptive motor responses during precision grip, *Exp. Brain Res.* **66**, 141–154 (1987).
31. N. Hogan, Impedance control: an approach to manipulation, *ASME J. Dyn. Syst. Meas. Control* **107**, 1–24 (1985).
32. F. Mussa-Ivaldi and N. Hogan, Integrable solutions of kinematic redundancy via impedance control, *Int. J. Robotics Res.* **10**, 481–491 (1991).
33. E. Burdet, R. Osu, D. Franklin, T. Milner and M. Kawato, The central nervous system stabilizes unstable dynamics by learning optimal impedance, *Nature* **414**, 446–449 (2001).
34. D. W. Franklin, R. Osu, E. Burdet, M. Kawato and T. E. Milner, Adaptation to stable and unstable environments achieved by combined impedance control and inverse dynamics model, *J. Neurophysiol.* **90**, 3270–3282 (2003).
35. S. Kajikawa, M. Saito, K. Ohba and H. Inooka, Analysis of human arm movement for catching a moving object, in: *Proc. Int. Conf. on Systems, Man, and Cybernetics* 2, pp. 698–703, Tokyo (1999).
36. M. Kaneko, M. Wada, H. Maekawa and K. Tanie, A new consideration on tendon tension control system of robot hands, in: *Proc. IEEE Int. Conf. on Robotics and Automation*, vol. 2, pp. 1028–1033, Sacramento, CA (1991).
37. A. H. Fagg, A model of muscle geometry for a two degree-of-freedom planar arm, *Technical Report* #00–03, Department of Computer Science, University of Massachusetts, Amherst, MA (2000).
38. J. E. Huber, N. A. Fleck and M. F. Ashby, The selection of mechanical actuators based on performance indices, *Math. Phys. Eng. Sci.* **453**, 2185–2205 (1997).

About the Authors



Emanuele Cattin received his Laurea Degree in Mechanical Engineering from the University of Padova in July 2003. In January 2004 he joined the Advanced Robotic Technology and System (ARTS) Lab at the Scuola Superiore Sant'Anna in Pisa as Research Assistant and since January 2005 he is PhD candidate in Robotics at University of Genova. He is currently involved in the NEUROBOTICS project at the ARTS Lab as mechanical designer of neuroscience robotic platforms and exoskeleton robotic systems for the human upper limb. His main research interests are in the fields of robotics, biomechanics, mechatronics, prosthesis and

biomechatronics.



Stefano Roccella received his Laurea degree in Aeronautical Engineering from the University of Pisa in 1999. In the same year he joined the Advanced Robotic Technology and System (ARTS) Laboratory of the Scuola Superiore Sant'Anna in Pisa as a Research Assistant. In March 2003 he started his PhD in Robotics at the University of Genova. Currently he is PhD in Robotics and Assistant Professor of Biomedical Robotics at Scuola Sant'Anna, where he is member of the ARTS Lab. His research interests are in the fields of biomedical robotics, rehabilitation engineering, biomechatronics, and MEMS design and development.



Nicola Vitiello received the MS degree in Biomedical Engineering (Magna Cum Laude) from the University of Pisa, in July 2006. He is currently Ph.D. student in Biorobotics, Scuola Superiore Sant'Anna, Pisa. He conducts his research activities at the Advanced Robotic Technology and System (ARTS) Laboratory of the Scuola Superiore Sant'Anna. His current research interests include the development of control algorithms for biorobotics platforms for investigating neuroscience issues.



Irene Sardellitti received the MS degree in Biomedical Engineering (Cum Laude) from Campus Bio-Medico, Rome, in 2004. She is currently a PhD candidate in Bioengineering, Scuola Superiore Sant'Anna, Pisa. She has been a Visiting Student in Khatib's Manipulation Group, Stanford University, since 2006.

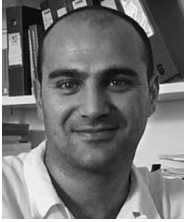
Her current research interests include system identification, advanced modeling and control of pneumatic artificial muscles, and hybrid actuation for human centered robotic manipulator design.



Panagiotis K. Artemiadis received the Diploma in mechanical engineering in 2003 from the National Technical University of Athens, Greece, where he is currently working towards the PhD degree. His research interest include neural control of robots, brain-machine interfaces, orthotic and prosthetic robotics and neural decoding. He is a regular reviewer of a number of conferences, while he is working in projects funded by the European Commission and the Greek secretariat for Research & Technology. He is a student member of IEEE and the Technical Chamber of Greece.



Pierpaolo Vacalebri received the Bachelor degree in Biomedical Engineering at the University of Pisa in 2007. From 2000 to 2004, he was a Research Assistant at the Applied Research Center on Rehabilitation Engineering, originated by a joint initiative promoted by INAIL and Scuola Superiore Sant'Anna, Pisa, where he was engaged in many projects related to design and development of human/machine interfaces, biomechatronic prostheses and robotic hands. Currently, he is with the Advanced Robotics Technology and Systems (ARTS) Laboratory of the Scuola Superiore Sant'Anna where he has been involved in the NEUROBOTICS Integrated Project, developing the electronics of a robotic arm. His current research interests include biomechatronics, and in particular the wireless protocols, telemetry and remote controls.



Fabrizio Vecchi received the university degree (Laurea) in Electrical Engineering from the University of Pisa, Italy, in 1999 and the PhD in Robotics from the University of Genova in 2003. He is a Post-Doc Research Scientist at the Advanced Robotic Technology and System (ARTS) Laboratory of Scuola Superiore Sant'Anna. His research interests are in the fields of biomechanics, rehabilitation engineering and neuro-robotics, and in particular in the design and development of human-machine interfaces, of biomechanical prosthetic and robotic hands, and of passive and active orthoses. Since 2004 he has been the Project Manager of the NEUROBOTICS Integrated Project (Fusion of Neuroscience and Robotics, IST-FET-2003-001917). He is member of the IEEE Engineering in Medicine and Biology Society and of the IEEE Robotics and Automation Society.



Maria Chiara Carrozza received the Laurea degree in physics from the University of Pisa, Pisa, Italy, in 1990. She received the PhD in Engineering at Scuola Superiore Sant'Anna in 1994. Since November 2006, she has been Full Professor of Biomedical Engineering and Robotics at Scuola Superiore Sant'Anna, Pisa, Italy. She is Director of Scuola Superiore Sant'Anna. She gives courses of Biomechanics and Rehabilitation Engineering to Master students of Biomedical Engineering at the University of Pisa and of Neuroscience and Robotics and Humanoid Robotics in the PhD programme of Biorobotics at Scuola Superiore Sant'Anna. She served as elected Member of the National Board of the Italian Association of Biomedical Engineering (Gruppo Nazionale di Bioingegneria).

She has been Visiting Professor at the Technical University of Wien, Austria with a graduate course entitled Biomechanics, and she is involved in the scientific management of the Italy-Japan joint laboratory for Humanoid Robotics ROBOCASA, Waseda University, Tokyo, Japan, where she is responsible for artificial hand design.

She served as Coordinator of the Advanced Robotics Technology and Systems Laboratory (<http://www.arts.sssup.it>), where more than 50 people are involved in research projects aimed at design, simulation and development of biomedical robots for rehabilitation engineering, functional support and humanoid robotics. She is a Member of IEEE RAS and EMBS societies, and the author of several scientific papers and international patents. In addition, she is promoting industrial innovation and start-up creation, she is Co-Founder of two spin-off companies of the Scuola Superiore Sant'Anna and she is a Member of their Administrative Boards.

She is currently Guest Co-Editor of the Special Issue on 'Robotic Platform for Research in Neuroscience' of *Advanced Robotics* and Guest Co-Editor of the Special Issue on 'Rehabilitation Robotics' on the *IEEE Transactions on Neural Systems and Rehabilitation Engineering*.



Kostas Kyriakopoulos received the Diploma in Mechanical Engineering with Honors from the National Technical University of Athens (NTUA), Greece, in 1985, and the MS and PhD in Electrical, Computer & Systems Engineering from Rensselaer Polytechnic Institute (RPI), Troy, NY, in 1987 and 1991, respectively. From 1988 to 1991 he did research at the NASA Center for Intelligent Robotic Systems for Space Exploration. Between 1991 and 1993 he was a Research Assistant Professor at the Electrical, Computer and Systems Engineering Department of RPI and the New York State Center for Advanced Technology in Automation and Robotics.

Since 1994 he has been with the Control Systems Laboratory of the Mechanical Engineering Department at NTUA, Greece, where he currently serves as a Professor and Director of the Computation Lab. His current interests are in the area of non-linear control systems applications in (i) sensor-based motion planning and control of multi-robotic systems: manipulators & vehicles (mobile, underwater and aerial) and (ii) micro-mechatronics. He was awarded the G. Samaras Award of Academic Excellence from NTUA, the Bodosakis Foundation Fellowship (1986–1989), the Alexander

Onassis Foundation Fellowship (1989–1990) and the Alexander Von Humboldt Foundation Fellowship (1993). He has published 150 papers in journals and refereed conferences; he serves on the Editorial Committee and as a regular reviewer of a number of journals and conferences, while he has served as an Administrative Member of a number of international conferences. He has contributed to a large number of projects funded by the European Commission and the Greek Secretariat for Research & Technology. He is a member of IEEE, EURON and the Technical Chamber of Greece.



Paolo Dario received the DE degree in Mechanical Engineering from the University of Pisa, Italy, in 1977. He is currently a Professor of Biomedical Robotics at the Scuola Superiore Sant'Anna, Pisa, Italy. He also teaches courses at the School of Engineering of the University of Pisa. He has been a Visiting Professor at many universities, including Brown University, USA, the Ecole Polytechnique Federale de Lausanne (EPFL), Switzerland, Waseda University, Japan, College de France, Paris, Ecole Normale Superieure de Cachan, France, and Zhejiang University, China. He was the Founder and is currently the Co-ordinator of the Advanced

Robotics Technologies and Systems (ARTS) Laboratory and the Center for Research in Microengineering Laboratory of the Scuola Superiore Sant'Anna, where he supervises a team of about 135 researchers and PhD students. He is also the Director of the Polo Sant'Anna Valdera, the Science Park of the Scuola Superiore Sant'Anna. His main research interests are in the fields of biorobotics, medical robotics, mechatronics and micro/nanoengineering. He has been and is the coordinator of many national and European projects, the editor of two books in robotics, and the author of more than 200 scientific papers (140 in ISI journals). He is Editor-in-Chief, Associate Editor and Member of the Editorial Board of many international journals. He served as President of the IEEE Robotics and Automation Society in the term 2002–03. He is a Fellow of the European Society on Medical and Biological Engineering, and a recipient of many honors and awards, such as the Joseph Engelberger Award. He is also a Member of the Board of the International Foundation of Robotics Research (IFRR).